ACS Catalysis

Research Article

Cite This: ACS Catal. 2018, 8, 8545–8552

pubs.acs.org/acscatalysis

Maximizing Solar Water Splitting Performance by Nanoscopic Control of the Charge Carrier Fluxes across Semiconductor–Electrocatalyst Junctions

Joseph Quinn, John Hemmerling, and Suljo Linic*

Department of Chemical Engineering, University of Michigan, Ann Arbor, Michigan 48109, United States

Supporting Information

ABSTRACT: Protective insulating layers between a semiconductor and an electrocatalyst enable otherwise unstable semiconductors to be used in photocatalytic water splitting. It is generally argued that in these systems the metal electrocatalyst must have work function properties that set a high inherent barrier height between the semiconductor and electrocatalyst and that the insulating layer should be as thin as possible. In this study we show that, for systems which suffer from inherently low barrier heights, the photovoltage can be significantly improved by tuning the thickness of the insulating layer. We demonstrate this in a case study of a system consisting of n-type silicon, a hafnium oxide protective layer (thickness 0–3 nm), and a Ni electrocatalyst. By optimizing the protective layer thickness, we observe increased efficiencies for photocatalytic oxygen evolution with a thick Ni electrocatalyst supported on n-Si. Our findings open avenues for the use of inexpensive electrocatalysts with favorable electrocatalytic and optical properties but poor work function characteristics.

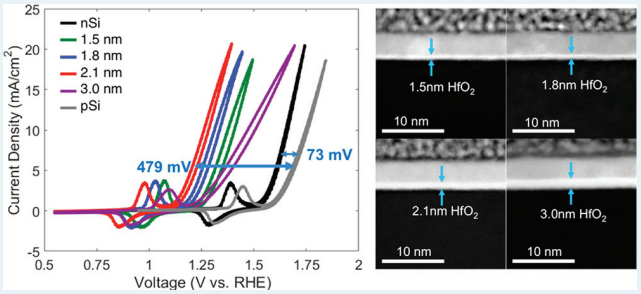

KEYWORDS: *water splitting, MIS junction, oxygen evolution, photoelectrocatalysis, photoanode*

Downloaded via UNIV OF MICHIGAN ANN ARBOR on September 1, 2018 at 17:50:20 (UTC).
See https://pubs.acs.org/sharingguidelines for options on how to legitimately share published articles.

Photocatalytic splitting of water into oxygen and hydrogen using sunlight is a critical bottleneck to the development of sustainable chemical conversion processes. The materials that have received the most attention for this application are hybrids that contain a semiconductor light absorber and an attached metal electrocatalyst that performs chemical transformations. While significant progress in the design of these multifunctional materials has been made, important inefficiencies have limited their viability. To mitigate these inefficiencies, strategies must be developed to (1) increase the total amount of absorbed solar irradiance by the semiconductor,[1,2] (2) improve the ability of the semiconductor to convert the absorbed light into chemically useful charge carriers (i.e., the charge carriers need to reach the reactive centers)[3−6], and (3) increase the activity of the attached electrocatalyst.[7] The first of these challenges is heavily dependent on the choice of semiconductor, which needs to have a band gap of between 1.1 and 2.0 eV to achieve optimal efficiencies for dual-semiconductor systems.[1,2] Almost all semiconductors with band gaps in this range (Si, GaAs, CdTe, etc.) are not stable under relevant photocatalytic conditions.[8] The main problem is that under anodic reaction conditions (the O_2-evolving electrodes), these materials are more readily oxidized and therefore degraded in comparison to the water reactant.

Recently, it has been demonstrated that these low band gap semiconductor photoanodes can be stabilized by the use of protective oxide layers. These structures often consist of a semiconductor layer, a protective insulator, and a metallic or metal oxide electrocatalyst (MIS system). While systems have been studied extensively in photovoltaic applications,[9−11] recently they have received renewed attention in photoelectrochemical applications where insulator layers are necessary to improve stability. Examples of insulator-protected photoelectrodes often employ a Si semiconductor covered with an Al_2O_3[12−15] and TiO_2[14,16−20] protective layer onto which a metal electrocatalyst was deposited. In these systems, the choice of the semiconductor, protective layer, and electrocatalyst materials affects the overall efficiencies. In general, it has been recognized that electrocatalysts, in addition to excellent electrocatalytic activity, need to have a work function such that the inherent electrocatalyst/semiconductor barrier height is high.[21] This means that for the water oxidation half-reaction (i.e., oxygen evolution reaction, OER), costly noble-metal electrocatalysts with high work functions, such as Ir (work function of 5.4–5.8 eV[22]), are desired. For electrocatalysts with acceptable water oxidation activities but poor work function characteristics, such as Ni[23,24] (surface anodized) and NiO_x[12,25] (the work function of Ni is ∼5.15 eV[26]), more elaborate structures have been used to achieve high efficiencies. These strategies include (1) forming a bimetallic layer with one metal setting the barrier height of

Received: May 18, 2018
Revised: July 30, 2018
Published: August 1, 2018

© XXXX American Chemical Society

DOI: 10.1021/acscatal.8b01929
ACS Catal. 2018, 8, 8545–8552

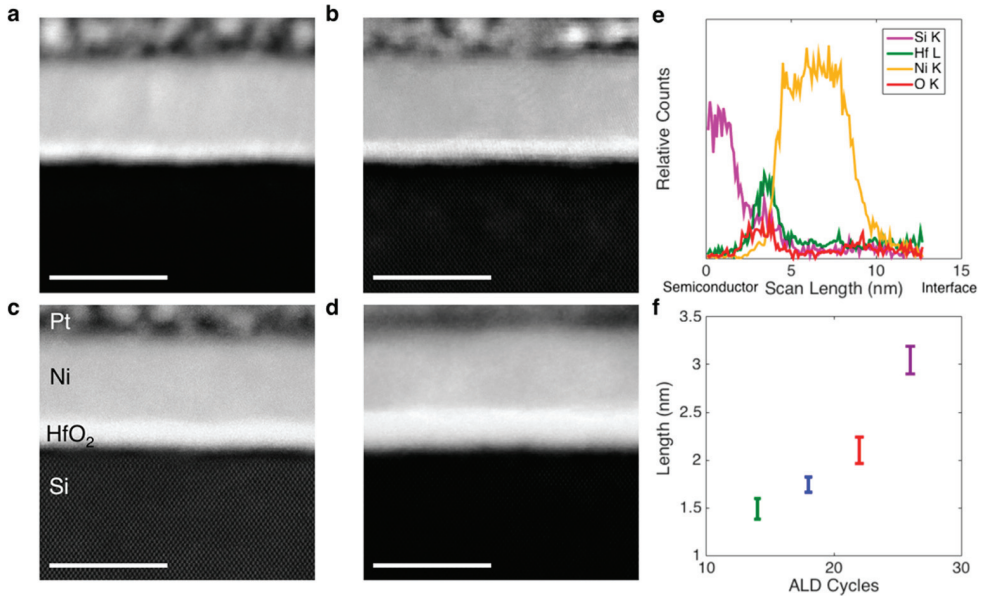

Figure 1. |Characterization of n-Si/HfO_2/Ni samples. Cross-sectional STEM images for (a) 14 cycles HfO_2, (b) 18 cycles HfO_2, (c) 22 cycles HfO_2, and (d) 26 cycles HfO_2. The layers are labeled in (c), and the scale bar represents 10 nm. The Pt layer was deposited to protect the Ni layer before ion milling. (e) Energy-dispersive X-ray spectroscopy (EDS) line scan of the n-Si/22c HfO_2/Ni cross-sectional sample. (f) HfO_2 thicknesses as a function of the number of HfO_2 ALD cycles measured from the TEM images. The error bars represent 1 standard deviation based on 10 different points across a sample.

the system and another functioning as the electrocatalyst[15,27] and (2) fabricating a p−n semiconductor junction beneath the insulator layer.[8,16,18] While these strategies can yield efficient photocatalyst systems, the fabrication complexity may increase costs. Additionally, these strategies are not easily implemented in some semiconductor systems, such as Cu_2O,[28] that are not conducive to forming efficient p−n heterojunctions.

It has also been argued that, in addition to the interface engineering required to optimize the semiconductor−electrocatalyst barrier height discussed above, the insulating protective layer should be as thin as possible.[18] The reason for this is that the transfer of photoexcited minority charge carriers should not be impeded by the insulating layer. Another study has shown an optimized photovoltage for moderate insulator thicknesses.[15] Both of these studies involved the use of high-barrier n-Si−Pt or n-Si−Ir junctions in order to suppress thermionic emission, which leads to recombination and a loss in photovoltage. In this report, we show that, by tuning the thickness of the insulating layer, even systems with moderate inherent barrier heights can achieve high efficiencies. We demonstrate that the thickness of the insulating protective layer is an important parameter that can be tuned to optimize the behavior of MIS photocatalyst systems: i.e., the thinnest protective layers do not necessarily produce the optimal performance. This is shown by the way of a concrete example where we employed n-type Si, a Ni electrocatalyst, and a HfO_2 protective layer as the MIS system for photocatalytic water oxidation. We note that it has been shown previously that the n-Si/Ni system exhibits a moderate barrier height, which limits the photovoltage and therefore the performance.[16] We show that, by tuning the thickness of the HfO_2 protective layer, we can maximize the performance of this system, generating a photovoltage that is 403 mV larger than that for the n-Si/Ni system without a protective layer and comparable to the highest reported value for similar systems that employ Ir electrocatalysts.[19] This strategy provides us with an additional way to optimize the performance of MIS photocatalysts, which can be used in place of the aforementioned p−n junction fabrication strategies. We support our experimental findings with a comprehensive model that captures the behavior of the system.

We fabricated layered Ni/HfO_2/Si MIS samples using atomic layer deposition (ALD). ALD is a widely recognized method to deposit pinhole-free, conformal layers with subnanometer precision. We note that several papers in water-splitting literature have reported atomic layer deposition (ALD) of insulator layers in the 1−3 nm range with no evidence of pinholes (see examples of atomic layer deposited TiO_2[17,29] and Al_2O_3.[13,15,30]). The thickness of the insulating HfO_2 layer was controlled by varying the number of ALD cycles.[31] Geometric characterization data in Figure 1 show that the synthesis yields layered Si/HfO_2/Ni structures. Figure 1a−d shows cross-sectional dark field scanning transmission electron micrographs (STEM) of the MIS samples with different HfO_2 thicknesses. The data in Figure 1e show the energy-dispersive X-ray spectroscopy (EDS) elemental line scan of a representative cross-sectional sample with clearly identifiable components of the layered nanostructures and defined boundaries between the different materials. Data in Figure 1f show the measured thickness of the HfO_2 layers in the MIS samples as a function of the number of ALD cycles used in the fabrication process. The data show that on average one ALD step results in 0.1 nm of deposited HfO_2. STEM images of the cross-sectional samples of the layered MIS materials demonstrated that the HfO_2 thickness was uniform for all of the imaged samples. Several additional cross sections were characterized for samples containing the thinnest insulator layer, and there were no detectable pinholes in any of the imaged samples, as shown in Figure S1.[13,15,17,29,30,31,32] While we made attempts to completely remove possible SiO_2 layers from the Si semiconductors, it is conceivable that very thin layers of SiO_2 persisted. If they existed, their effect on the

DOI: 10.1021/acscatal.8b01929
ACS Catal. 2018, 8, 8545−8552

MIS performance would be uniform across different MIS samples. Additional characterization data are given in the Supporting Information.

To evaluate the performance of these materials in the water oxidation reaction, we performed cyclic voltammetry (CV) measurements in a three-electrode setup in 1 M KOH saturated with oxygen using an ~100 mW/cm^2 halogen lamp (mimicking sunlight). The Methods section contains additional setup information. Data in Figure 2a show the measured

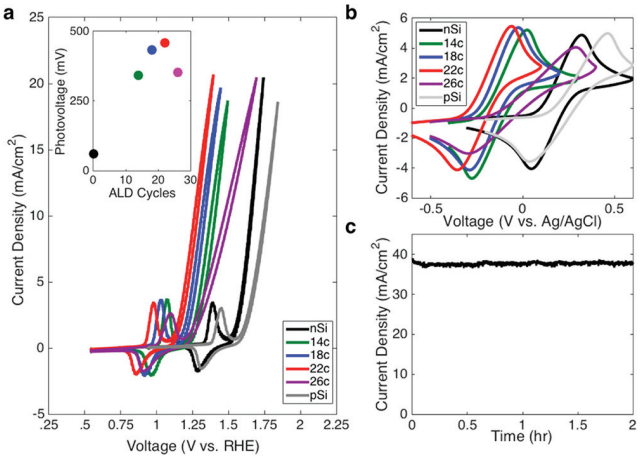

Figure 2. |Electrochemical performance of the n-Si/x-HfO_2/7 nm Ni samples. (a) Current−voltage response upon illumination in 1 M KOH for increasing HfO_2 thickness. The inset shows the measured photovoltage at 1 mA/cm^2 as a function of the HfO_2 ALD cycle number. From 0 to 22 ALD cycles (0−2.1 nm HfO_2) the photovoltage improves, but it decreases for greater HfO_2 thickness. (b) Cyclic voltammograms performed under illumination in 10 mM ferri-/ferrocyanide and 1 M KCl corroborating that photovoltage is optimized for moderate HfO_2 thickness. (c) Chronoamperogram for an n-Si/22 cycle HfO_2/Ni island sample showing that the HfO_2-protected n-Si is stable in 1 M KOH at a potential of 1.8 V vs RHE for 2 h of operation.

current (reaction rate) as a function of voltage (the potential of majority charge carriers with respect to reversible hydrogen electrode). In these experiments the redox waves prior to the onset of water oxidation correspond to the Ni^{2+}/Ni^{3+} oxidation peak (thick Ni electrocatalysts have been shown to form a nonpenetrating surface oxide,[23,24] which is shown in Figure S2). The data show that the performance improves considerably from 0 to 22 HfO_2 ALD cycles (0 to 2.1 nm) and decreases for greater thickness. Data in the inset in Figure 2a show the measured HfO_2-thickness-dependent photovoltage for various MIS samples. We defined photovoltage as the difference between the voltage measured at a current of 1 mA/cm^2 for the illuminated samples and the voltage for the p-Si/Ni control system. The data show that the photovoltage obtained for the n-Si/Ni system without the HfO_2 protective layer is very low (~76 mV), corroborating the low work function of Ni and a very poor n-Si/Ni barrier height. On the other hand, the photovoltage significantly improves with the introduction of the HfO_2 protective layer, reaching a maximum of 479 mV for the 2.1 nm HfO_2 layer and then dropping for greater HfO_2 thicknesses. This observed volcano behavior of the photovoltage for the MIS samples as a function of the protective layer thickness suggests that there is an optimal thickness of the insulating layers and that the highest performance is not achieved by the minimum oxide layer thickness. The photovoltage measured for the HfO_2 thickness of 2.1 nm is the highest reported for a thick Ni electrocatalyst on Si.[23,24]

To further characterize the behavior of these MIS photocatalyst systems, the samples were tested as photocatalysts for the ferro-/ferricyanide redox reaction. This redox reaction is a one-electron-transfer process that exhibits no overpotential losses, and therefore it can be used to deconvolute photovoltage generated by the system from the electrochemical overpotential losses, which are significant for the OER kinetics on Ni. Data in Figure 2b show the current−voltage response of the photocatalysts in 10 mM ferri-/ferrocyanide and 1 M KCl under 100 mW/cm^2 broad-band light source illumination. For this reaction photovoltage is defined as the difference in $E_{1/2}$ between the n-Si/x-HfO_2/Ni and the p-Si/Ni samples, where $E_{1/2}$ is the midpoint voltage between the oxidation and reduction peak potentials. The data are consistent with the OER results indicating that the photovoltage improves significantly as the HfO_2 thickness is increased from 0 to 2.1 nm and decreases for greater HfO_2 thickness.[33,34−36]

Since the presence of semiconductor/metal/electrolyte three phase boundary in these systems introduces additonal level of compelxities[16,33−36], which can compromis the system stability, we also exemined the viability of the HfO_2 protective layer (we note that this material has not been used previously as a protective layer) in samples consisting of the Si and HfO_2 layers covered by Ni islands (the Ni islands were 3 μm diameter and 5 nm thickness). A detailed description of sample fabrication is provided in Methods. A scanning electron micrograph of the nSi/HfO_2/Ni island sample is shown in Figure S3. Chronoamperometry measurements were performed to examine the stability of the HfO_2 protective layer. Chronoamperometry data in Figure 2c obtained in the photolimiting current regime (1.8 V vs RHE) show that the current is stable for over 2 h of continuous operation, indicating that the HfO_2 layer provides a high degree of protection. This is not surprising, considering the demonstrated stability of this material under highly oxidizing conditions.[37] The demonstrated stability also indicates that there are no significant pinholes in the HfO_2 layer, as pinholes would enable direct contact between the electrolyte and the Si, resulting in immediate degradation.

The data in Figure 2 show that the thickness of the insulating HfO_2 layer can be tuned to maximize the performance of the MIS photocatalysts. To shed light on the observed behavior of the Si/HfO_2/Ni layered photocatalysts, we developed a mathematical model, inspired by recent works of Mills et al.,[38] to model the performance of these systems as a function of the thickness of the insulating layers. A detailed description of the model is provided in the Supporting Information. In short, numerical methods are used to solve Poisson's equation and charge carrier continuity equations for both charge carriers iteratively to determine potential and charge carrier concentration profiles across an illuminated semiconductor. The Butler−Volmer equation is used to model the rate of the electrocatalytic reaction on Ni. The rate of charge transfer between the Si semiconductor and Ni catalysts through the insulating HfO_2 layer represents a boundary condition to the continuity equation. This is an important physical parameter, which is described using the equation (see the Supporting Information and ref 38 for the justification)

DOI: 10.1021/acscatal.8b01929
ACS Catal. 2018, 8, 8545−8552

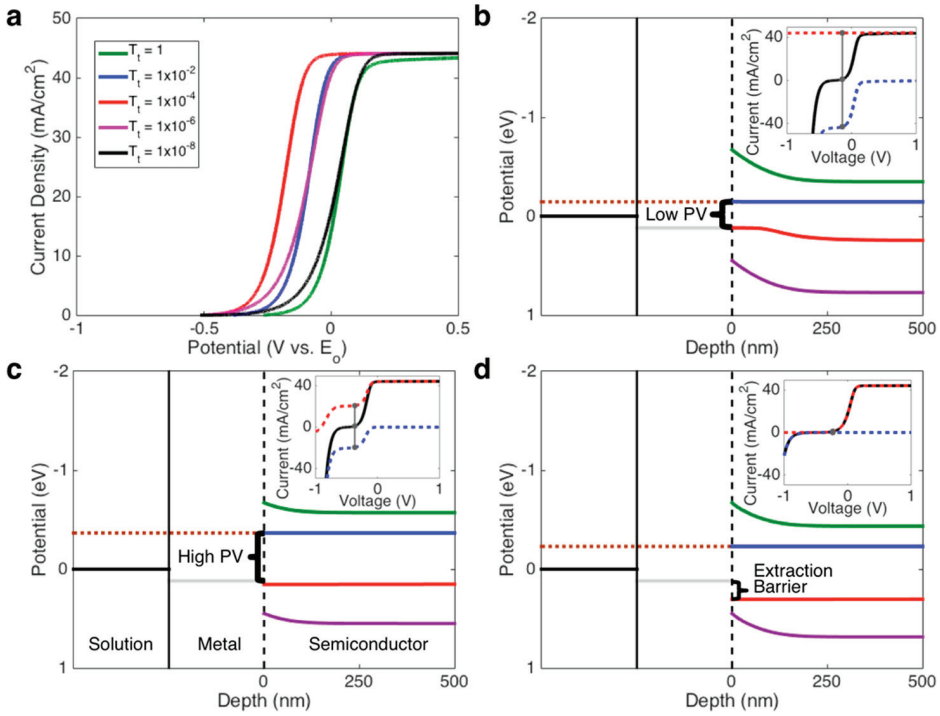

Figure 3. |Model results for variable tunneling probabilities. (a) Modeled current−voltage response showing optimized performance for moderate tunneling probabilities, and therefore charge transfer rates. The potential is measured vs the solution potential E_o. (b−d) Calculated band diagrams at 1 mA/cm^2 for high ($T_t = 1$), moderate ($T_t = 1 \times 10^{-4}$), and low ($T_t = 1 \times 10^{-8}$) tunneling probabilities. The green and violet lines are the conduction and valence bands, the blue and red lines represent the electron and hole quasi-Fermi levels, the horizontal black line is the potential of the redox couple in solution, the brown dashed line is the applied potential (with respect to the potential of the redox couple in solution), and the gray line is the electrocatalyst potential. The vertical dashed line marks the insulator layer at the semiconductor−metal boundary. The insets represent the individual charge carrier fluxes as a function of applied potential for each tunneling probability. The blue and red dashed lines represent the electron and hole currents, respectively. The black line marks the net current. The gray dot represents the point at 1 mA/cm^2 net current, where the band diagrams are calculated. The gray vertical lines highlight electron and hole flux overlap leading to recombination, with longer lines indicating a higher electron/hole recombination current.

$$J = k_p T_t (p_s - \overline{p}_s) - k_n T_t (n_s - \overline{n}_s) \quad (1)$$

where k_p is the charge transfer rate coefficient for holes (mA cm), k_n is the charge transfer rate coefficient for electrons (mA cm), p_s is the hole concentration at the illuminated semiconductor surface, $\overline{p}_s$ is the equilibrium surface hole concentration (at open circuit voltage in the dark), n_s is the surface electron concentration, and $\overline{n}_s$ is the equilibrium surface electron concentration. T_t describes the probability that the charge carriers tunnel through the insulator layer. It has been established that charge transfer rates for tunneling through an oxide insulator—previous studies have shown that HfO_2 transfers charge via a tunneling mechanism—are proportional to tunneling probability, as shown in eq 2[39]

$$T_t \approx \exp(-\alpha_t d\sqrt{\phi_t}) \quad (2)$$

where α_t is a constant that is a function of the electron effective mass in the insulator, d is insulator thickness (Å), and ϕ_t is a tunneling barrier described as the difference between the band edges of the semiconductor and insulator layer (V). Zhu et al. experimentally determined the value of ϕ_t for a metal−HfO_2−Si MIS system to be 1.1 eV.[40] With this value of the tunneling barrier, the tunneling probabilities vary by a few orders of magnitude for the HfO_2 thicknesses explored in our studies. In our simulations, charge transfer rate coefficients of k_n, $k_p = 1 \times 10^{-12}$ mA cm were taken as a baseline (this value corresponds to fast transfer with no insulator[38]) and the tunneling parameter T_t was adjusted from 1 to 1×10^{-8}. This range corresponds to an insulator thickness range of ∼0−5 nm. Additional justification is provided in the Supporting Information.

Data in Figure 3a show the calculated current−voltage behavior of the system as a function of the tunneling probability, which as discussed above modifies charge transfer rates. The data in Figure 3a support our experimental results, showing that the performance of the system is a strong function of the tunneling probability and therefore the thickness of the protective insulating layer with intermediate tunneling probabilities (charge transfer rates) leads to the optimal performance.

Analysis of the computed band diagrams in Figure 3b−d sheds light on the underlying reasons for the observed thickness-dependent performance of these materials. The representative band diagrams were computed for a current of 1 mA/cm^2 and therefore a constant voltage of the Ni electrocatalyst. In the limit of very high tunneling probabilities (Figure 3b), which is consistent with a nonexistent or very low HfO_2 thickness, under illumination the minority charge carriers are rapidly exchanged between the semiconductor and electrocatalyst. This leads to equilibration in the potential of the minority charge carriers at the semiconductor surface and the electrocatalyst potential. Due to the inherently low barrier height of the Ni/n-Si junction, characterized by similar Fermi level positions, under the conditions of high tunneling

DOI: 10.1021/acscatal.8b01929
ACS Catal. 2018, 8, 8545−8552

probability there is also a significant leakage of the majority charge carriers into the metal electrocatalyst, leading to fast parasitic charge recombination in the metal. As a consequence, these losses lead to low photovoltage and therefore poor performance.

This situation can be improved by designing systems with inherently lower charge transfer rates (Figure 3c). One way to accomplish this is to introduce thin insulating layers between the semiconductor and metal electrocatalyst. While decreasing the tunneling probability decreases the rate of both minority and majority charge carriers, it is possible to have a situation where the minority charge carriers are still at the equilibrium potential (or close to it) with the electrocatalyst (i.e., the exchange rate on the minority charge carriers with the electrocatalyst is still relatively fast), while the leakage current of the majority charge carriers to the electrocatalyst is significantly lowered. This is an ideal scenario, as it leads to minimal charge carrier recombination rates and efficient conversion of the minority charge carriers into the reaction rate. After this point, any further decreases to the tunneling probability do not increase the photovoltage (Figure 3d) but rather lead to voltage losses due to the presence of the barrier for the extraction of the minority charge carriers from the semiconductor to the electrocatalyst.

Another way to describe our experimental observation is to focus on the fluxes of majority and minority charge carriers across the semiconductor−metal interfaces (shown as the function of the applied potential in the insets in Figure 3b−d). At identical current densities (for example, 1 mA/cm^2), the net charge carrier fluxes (flux of holes−flux of electrons) through the insulator to the catalyst are identical. However, if the fluxes of individual majority and minority carrier currents are high (much higher than the net reaction rate), there will be large recombination currents in the metal, resulting in low photovoltage. If both charge carrier currents are decreased, the recombination current in the metal can be reduced without sacrificing the total net current. If the tunneling probabilities are decreased too much, the minority charge carrier currents become very small, which means external voltage must be applied in order to achieve the same net current.

This analysis suggests that, by engineering nanostructures that can control the fluxes of charge carriers from the semiconductor to the electrocatalyst, we can improve the performance of these layered photocatalyst materials. In this particular case, we were able to accomplish this by tuning the thickness of the insulating protective layer between the electrocatalyst and semiconductor. The enhanced photovoltage can further be explained in terms of a conventional description of a semiconductor/electrocatalyst system, which is often based on using an ideal diode approximation to describe the behavior of a semiconductor light absorber. The illuminated ideal diode equation can be expanded to account for MIS junctions by applying the tunneling probability term:[10]

$$J(V) = -J_s \exp(-\alpha_t d\sqrt{\phi_t})\left\{\exp\left(\frac{-qV}{kT}\right) - 1\right\} + J_{ph}$$

$$J_s = AT^2 \exp\left(\frac{-q\phi}{kT}\right) \quad (3)$$

In this equation J_s is the reverse saturation current, A represents Richardson's constant, ϕ represents the barrier height, k is the Boltzmann constant, T is temperature, J_{ph} is the photolimited current density, and V is the applied voltage (voltage for majority charge carriers with respect to the solution potential). For the case of $J(V) = 0$, and in the limit of $J_{ph} \gg J_s$, eq 3 can be solved for the open circuit voltage (V_{oc}), which is essentially a measure of photovoltage at zero net current.

$$-V_{oc} \approx \frac{kT}{q}\ln\frac{J_{ph}}{AT^2} + \phi + \frac{kT}{q}\alpha_t d\sqrt{\phi_t} \quad (4)$$

Equation 4 suggests that, for a given barrier height and photolimited current density, there should be a linear correlation between the open circuit voltage (i.e., the photovoltage) and the thickness of the insulator layer. Data in Figure 2a (including the inset) and Figure 2b show the measured photovoltage as the function of the thickness of the HfO_2 layer. The measured linear relationship between the photovoltage and the HfO_2 thickness clearly supporta our thesis that the photovoltage is tuned by tuning the thickness of the insulator. We note that eqs 3 and 4 do not apply for very thick insulator structures, since the low tunneling probability results in significant additional losses in potential which are required to force the minority charge carriers through the insulator. These losses are not captured in the ideal diode equation, and they are the reasons for the declining performance of the materials for HfO_2 layers thicker than ~2.1 nm (>22 ALD cycles).

Another way to test whether by tuning the thickness of the inert oxide layer we are essentially adjusting the open circuit voltage is to measure the flux of majority charge carriers in the dark as a function of applied potential. In this case, if the insulator thickness is increased, then lower applied potentials (higher energy of electrons) are required to cross over the barrier into the solution. This effect can be seen from eq 3 by removing the J_{ph} term (i.e., dark operation). To test this experimentally, we monitored the reduction of the 50/50 ferri-/ferrocyanide solution under dark conditions. The measurements were performed in a vigorously stirred solution to avoid the limitations due to the transfer of the reactants from the solution to the surface of the photocatalyst. The CV data in Figure 4 show that, for greater thicknesses of HfO_2,

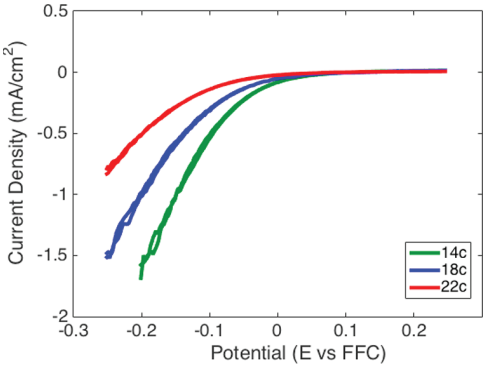

Figure 4. |Majority carrier currents for increasing insulator thickness. Current−voltage response of the n-Si/HfO_2/Ni electrodes in a vigorously stirred solution of 50-/50 ferri/ferrocyanide (FFC) for increasing ALD cycle number. These measurements were performed in the dark, causing majority carriers (electrons) to perform the cathodic reaction. For an increasing number of ALD cycles (insulator thickness 0−2.1 nm HfO_2), more negative potentials are required to induce the FFC reduction reaction, indicating that the flux of majority carriers is impeded by the increase in insulator thickness.

DOI: 10.1021/acscatal.8b01929
ACS Catal. 2018, 8, 8545−8552

more negative potentials (higher energy electrons) are required to induce the reduction reaction, which is consistent with our hypothesis.

In conclusion, our analysis suggests that by engineering insulating layers between a semiconductor and an electrocatalyst we can improve not only the stability of photocatalytic systems in water oxidation but also the photovoltage obtained by these systems. We demonstrate that this is accomplished by the insulator-induced tuning of the fluxes of charge carriers from the semiconductor to the electrocatalyst, which can minimize charge carrier recombination rates. The observed behavior should apply for all MIS systems characterized by relatively poor inherent barrier heights (low work function difference between the semiconductor and electrocatalyst or poor electronic properties of the semiconductor/electrocatalyst interface) that employ insulators which conduct charge carriers via the tunneling mechanism. This strategy can be used to expand the phase space of potentially useful semiconductor−electrocatalyst pairings for photocatalytic transformations by allowing for the use of active electrocatalysts with poor work function characteristics or for the use of semiconductors that are not conducive for p−n junction fabrication. The MIS systems that have large inherent semiconductor/electrocatalyst barrier heights will not benefit from this approach, and these should observe declining photovoltage for increasing insulator thickness, as reported previously for the nSi−TiO_2−Ir system.[18]

METHODS

Sample Fabrication. Moderately doped n-Si (ρ = 1−10 Ω cm) (Silicon Valley Microelectronics) and p-Si (ρ = 1−3 Ω cm) (Silicon Resource Company) were cleaned with Nano-Strip (a commercial piranha solution) for 10 min at 60 °C and dipped in buffered hydrofluoric acid for 1 min. Thin (1−3 nm) HfO_2 layers were deposited via atomic layer deposition (ALD) on the Si wafers using an Oxford Instruments OpAL Atomic Layer Deposition System. In this process the ALD chamber is pumped down to 25 mT and preheated to 275 °C. The substrate is exposed to a number of ALD cycles in order to deposit a monolayer of HfO_2. An ALD cycle consists of (1) a precursor dose of tetrakis(ethylmethylamino)hafnium (TEMAH) for 800 ms followed by a purge and (2) a 30 ms H_2O dose followed by a purge. The pulses were performed at ∼250 mT. After the ALD process a 7 nm Ni layer was deposited on the HfO_2-coated wafers at a rate of 1 Å/s at a base pressure of 2 × 10^{-6} Torr using electron beam evaporation. The wafers were diced into 13 × 13 mm squares. For the Ni island samples the HfO_2 layer was deposited by the same procedure as that described above. The HfO_2 samples were then spin-coated in SPR 220 (Dow) and baked at 115 °C for 90 s. The wafers were exposed to light through a mask with a GCA AS200 AutoStep and developed in order to make 3 μm diameter holes in the photoresist layer. The wafer was then subjected to an O_2 plasma descum to remove any remaining photoresist residue in the holes. The Ni evaporation procedure was the same as that described above. After Ni deposition the wafer was dipped in acetone to lift off the photoresist.

Sample Characterization. Scanning transmission electron microscopy (STEM) and energy-dispersive X-ray spectroscopy (EDS) was performed with a JEOL 2100 probe-corrected analytical electron microscope with an accelerating voltage of 100 kV. The samples were prepared via focused ion milling with a FEI Nova 200 nanolab SEM/FIB apparatus.

HfO_2 Thickness Measurements. Bright field STEM images were used to measure HfO_2 thickness. The HfO_2/Ni boundary is marked by a change in contrast/grain structure. This boundary was verified with EDS elemental mapping and EDS line scans. The thicknesses were measured with IMAGEJ.

Electrochemical Testing. Electrochemical measurements were performed in a three-electrode cell. A 1 M KOH (Fischer Scientific) electrolyte was used for the water oxidation measurements. Samples were illuminated with an ∼100 mW/cm^2 halogen lamp, the intensity of which was measured with a thermopile detector. p-type samples were measured in the dark. A Pt counter electrode and an Hg/HgO reference electrode were used. The scan rate was 100 mV/s. Oxygen was bubbled into the electrolyte throughout the experiments. The electrodes were cycled 10 times before measurements to ensure current stability. The following equation was used in order to convert from the Hg/HgO reference to the RHE at pH 14:

$$V_{RHE} = V_{Hg/HgO} + 0.118 + 0.0591 \times pH$$

The ferri-/ferrocyanide solution was made up of 10 mM potassium hexacyanoferrate(II) trihydrate, 10 mM potassium hexacyanoferrate(III) (EMD Millipore), and 1 M KCl (Fischer Scientific). This study reports uncorrected values of the Ag/AgCl reference for the samples tested in ferri-/ferrocyanide. The samples were housed in a 3D-printed electrode. The back contacts of the samples were scratched with a diamond scribe to remove the native oxide, and a gallium−indium eutectic was applied to ensure ohmic contact. The back contacts were then pressed against a copper plate. The samples were exposed toa light source via a 0.264 cm^2 aperture. An O-ring pressed to the sample surface prevented the electrolyte from leaking to the back contact.

ASSOCIATED CONTENT

Supporting Information

The Supporting Information is available free of charge on the ACS Publications website at DOI: 10.1021/acscatal.8b01929.

Microscopy characterization, postexperiment characterization, and detailed modeling description (PDF)

AUTHOR INFORMATION

Corresponding Author

*E-mail for S.L.: linic@umich.edu.

ORCID

Joseph Quinn: 0000-0002-8742-7052

Author Contributions

J.Q. and S.L. designed the experiments. J.Q. synthesized the samples, performed the electrochemical testing, performed materials characterization, and developed the finite difference model. J.H. developed the analytical model for the comparison analysis. All authors assisted in the preparation of the manuscript.

Notes

The authors declare no competing financial interest.

ACKNOWLEDGMENTS

This work was primarily supported by the National Science Foundation (NSF) (CBET-1803991, CBET-1437601, and CBET- 1702471). Secondary support for the development of analytical tools used to analyze the catalytic properties of

DOI: 10.1021/acscatal.8b01929
ACS Catal. 2018, 8, 8545−8552

materials was provided by the US Department of Energy, Office of Basic Energy Science, Division of Chemical Sciences (FG-02-05ER15686). Secondary support for the fabrication of the samples and microscopy was provided by the NSF (CBET-1436056 and CBET-1437601). S.L. also acknowledges the partial support of Technische Universität München−Institute for Advanced Study, funded by the German Excellence Initiative and the European Union Seventh Framework Programme under grant agreement no. 291763.

REFERENCES

(1) Seitz, L. C.; Chen, Z.; Forman, A. J.; Pinaud, B. A.; Benck, J. D.; Jaramillo, T. F. Modeling Practical Performance Limits of Photoelectrochemical Water Splitting Based on the Current State of Materials Research. *ChemSusChem* **2014**, *7* (5), 1372−1385.
(2) Chen, Y.; Hu, S.; Xiang, C.; Lewis, N. S. A Sensitivity Analysis to Assess the Relative Importance of Improvements in Electrocatalysts, Light Absorbers, and System Geometry on the Efficiency of Solar-Fuels Generators. *Energy Environ. Sci.* **2015**, *8*, 876.
(3) Ingram, D. B.; Linic, S. Water Splitting on Composite Plasmonic-Metal/Semiconductor Photoelectrodes: Evidence for Selective Plasmon-Induced Formation of Charge Carriers near the Semiconductor Surface. *J. Am. Chem. Soc.* **2011**, *133* (14), 5202−5205.
(4) Christopher, P.; Ingram, D. B.; Linic, S. Enhancing Photochemical Activity of Semiconductor Nanoparticles with Optically Active Ag Nanostructures: Photochemistry Mediated by Ag Surface Plasmons. *J. Phys. Chem. C* **2010**, *114* (19), 9173−9177.
(5) Ingram, D. B.; Christopher, P.; Bauer, J. L.; Linic, S. Predictive Model for the Design of Plasmonic Metal/Semiconductor Composite Photocatalysts. *ACS Catal.* **2011**, *1* (10), 1441−1447.
(6) Hernley, P. A.; Chavez, S. A.; Quinn, J. P.; Linic, S. Engineering the Optical and Catalytic Properties of Co-Catalyst/Semiconductor Photocatalysts. *ACS Photonics* **2017**, *4* (4), 979−985.
(7) Lewis, N. S. Research Opportunities to Advance Solar Energy Utilization. *Science* **2016**, *351* (6271), aad1920.
(8) Hu, S.; Lewis, N. S.; Ager, J. W.; Yang, J.; McKone, J. R.; Strandwitz, N. C. Thin-Film Materials for the Protection of Semiconducting Photoelectrodes in Solar-Fuel Generators. *J. Phys. Chem. C* **2015**, *119* (43), 24201−24228.
(9) Singh, R.; Green, M. A.; Rajkanan, K. Review of Conductor-Insulator-Semiconductor (CIS) Solar Cells. Sol. *Sol. Cells* **1981**, *3* (2), 95−148.
(10) Card, H. C.; Rhoderick, E. H. Studies of Tunnel MOS Diodes I. Interface Effects in Silicon Schottky Diodes. *J. Phys. D: Appl. Phys.* **1971**, *4* (10), 1589.
(11) Olsen, L. C. Model Calculations for Metal-Insulator-Semiconductor Solar Cells. *Solid-State Electron.* **1977**, *20* (9), 741−751.
(12) Park, M.-J.; Jung, J.-Y.; Shin, S.-M.; Song, J.-W.; Nam, Y.-H.; Kim, D.-H.; Lee, J.-H. Photoelectrochemical Oxygen Evolution Improved by a Thin Al2O3 Interlayer in a NiOx/n-Si Photoanode. *Thin Solid Films* **2016**, *599*, 54−58.
(13) Digdaya, I. A.; Adhyaksa, G. W. P.; Trześniewski, B. J.; Garnett, E. C.; Smith, W. A. Interfacial Engineering of Metal-Insulator-Semiconductor Junctions for Efficient and Stable Photoelectrochemical Water Oxidation. *Nat. Commun.* **2017**, *8*, 15968.
(14) Scheuermann, A. G.; Kemp, K. W.; Tang, K.; Lu, D. Q.; Satterthwaite, P. J.; Ito, T.; Chidsey, C. E. D.; McIntyre, P. C. Conductance and Capacitance of Bilayer Protective Oxides for Silicon Water Splitting Anodes. *Energy Environ. Sci.* **2016**, *9* (2), 504−516.
(15) Digdaya, I. A.; Trześniewski, B. J.; Adhyaksa, G. W. P.; Garnett, E. C.; Smith, W. A. General Considerations for Improving Photovoltage in Metal-Insulator-Semicondutor Photoanodes. *J. Phys. Chem. C* **2018**, *122*, 5462.
(16) Hu, S.; Shaner, M. R.; Beardslee, J. A.; Lichterman, M.; Brunschwig, B. S.; Lewis, N. S. Amorphous TiO2 Coatings Stabilize Si, GaAs, and GaP Photoanodes for Efficient Water Oxidation. *Science* **2014**, *344* (6187), 1005−1009.
(17) Chen, Y. W.; Prange, J. D.; Dühnen, S.; Park, Y.; Gunji, M.; Chidsey, C. E. D.; McIntyre, P. C. Atomic Layer-Deposited Tunnel Oxide Stabilizes Silicon Photoanodes for Water Oxidation. *Nat. Mater.* **2011**, *10* (7), 539−544.
(18) Scheuermann, A. G.; Lawrence, J. P.; Kemp, K. W.; Ito, T.; Walsh, A.; Chidsey, C. E. D.; Hurley, P. K.; McIntyre, P. C. Design Principles for Maximizing Photovoltage in Metal-Oxide-Protected Water-Splitting Photoanodes. *Nat. Mater.* **2016**, *15* (1), 99−105.
(19) Scheuermann, A. G.; Lawrence, J. P.; Meng, A. C.; Tang, K.; Hendricks, O. L.; Chidsey, C. E. D.; McIntyre, P. C. Titanium Oxide Crystallization and Interface Defect Passivation for High Performance Insulator-Protected Schottky Junction MIS Photoanodes. *ACS Appl. Mater. Interfaces* **2016**, *8* (23), 14596−14603.
(20) McDowell, M. T.; Lichterman, M. F.; Carim, A. I.; Liu, R.; Hu, S.; Brunschwig, B. S.; Lewis, N. S. The Influence of Structure and Processing on the Behavior of TiO2 Protective Layers for Stabilization of N-Si/TiO2/Ni Photoanodes for Water Oxidation. *ACS Appl. Mater. Interfaces* **2015**, *7* (28), 15189−15199.
(21) Walter, M. G.; Warren, E. L.; McKone, J. R.; Boettcher, S. W.; Mi, Q.; Santori, E. A.; Lewis, N. S. Solar Water Splitting Cells. *Chem. Rev.* **2010**, *110* (11), 6446−6473.
(22) Strayer, R. W.; Mackie, W.; Swanson, L. W. Work Function Measurements by the Field Emission Retarding Potential Method. *Surf. Sci.* **1973**, *34* (2), 225−248.
(23) Kenney, M. J.; Gong, M.; Li, Y.; Wu, J. Z.; Feng, J.; Lanza, M.; Dai, H. High-Performance Silicon Photoanodes Passivated with Ultrathin Nickel Films for Water Oxidation. *Science* **2013**, *342* (6160), 836−840.
(24) Laskowski, F. A. L.; Nellist, M. R.; Venkatkarthick, R.; Boettcher, S. W. Junction Behavior of N-Si Photoanodes Protected by Thin Ni Elucidated from Dual Working Electrode Photoelectrochemistry. *Energy Environ. Sci.* **2017**, *10* (2), 570−579.
(25) Sun, K.; McDowell, M. T.; Nielander, A. C.; Hu, S.; Shaner, M. R.; Yang, F.; Brunschwig, B. S.; Lewis, N. S. Stable Solar-Driven Water Oxidation to O2(g) by Ni-Oxide-Coated Silicon Photoanodes. *J. Phys. Chem. Lett.* **2015**, *6* (4), 592−598.
(26) Eastman, D. E. Photoelectric Work Functions of Transition, Rare-Earth, and Noble Metals. *Phys. Rev. B* **1970**, *2* (1), 1−2.
(27) Esposito, D. V.; Levin, I.; Moffat, T. P.; Talin, A. A. H2 Evolution at Si-Based Metal−Insulator−Semiconductor Photoelectrodes Enhanced by Inversion Channel Charge Collection and H Spillover. *Nat. Mater.* **2013**, *12* (6), 562−568.
(28) Wilson, S. S.; Bosco, J. P.; Tolstova, Y.; Scanlon, D. O.; Watson, G. W.; Atwater, H. A. Interface Stoichiometry Control to Improve Device Voltage and Modify Band Alignment in ZnO/Cu2O Heterojunction Solar Cells. *Energy Environ. Sci.* **2014**, *7* (11), 3606−3610.
(29) Scheuermann, A. G.; Prange, J. D.; Gunji, M.; Chidsey, C. E. D.; McIntyre, P. C. Effects of Catalyst Material and Atomic Layer Deposited TiO 2 Oxide Thickness on the Water Oxidation Performance of Metal−Insulator−Silicon Anodes. *Energy Environ. Sci.* **2013**, *6* (8), 2487−2496.
(30) Choi, M. J.; Jung, J.-Y.; Park, M.-J.; Song, J.-W.; Lee, J.-H.; Bang, J. H. Long-Term Durable Silicon Photocathode Protected by a Thin Al2O3/SiOx Layer for Photoelectrochemical Hydrogen Evolution. *J. Mater. Chem. A* **2014**, *2* (9), 2928−2933.
(31) Ritala, M.; Leskelä, M. Atomic Layer Epitaxy - a Valuable Tool for Nanotechnology? *Nanotechnology* **1999**, *10* (1), 19.
(32) Marichy, C.; Bechelany, M.; Pinna, N. Atomic Layer Deposition of Nanostructured Materials for Energy and Environmental Applications. *Adv. Mater.* **2012**, *24* (8), 1017−1032.
(33) Bae, D.; Seger, B.; Vesborg, P. C. K.; Hansen, O.; Chorkendorff, I. Strategies for Stable Water Splitting via Protected Photoelectrodes. *Chem. Soc. Rev.* **2017**, *46* (7), 1933−1954.
(34) Laursen, S.; Linic, S. Strong Chemical Interactions Between Au and Off-Stoichiometric Defects on TiO2 as a Possible Source of Chemical Activity of Nanosized Au Supported on the Oxide. *J. Phys. Chem. C* **2009**, *113* (16), 6689−6693.

DOI: 10.1021/acscatal.8b01929
ACS Catal. 2018, 8, 8545−8552

(35) Mukherjee, J.; Linic, S. First-Principles Investigations of Electrochemical Oxidation of Hydrogen at Solid Oxide Fuel Cell Operating Conditions. *J. Electrochem. Soc.* **2007**, *154* (9), B919−B924.
(36) Ingram, D. B.; Linic, S. First-Principles Analysis of the Activity of Transition and Noble Metals in the Direct Utilization of Hydrocarbon Fuels at Solid Oxide Fuel Cell Operating Conditions. *J. Electrochem. Soc.* **2009**, *156* (12), B1457−B1465.
(37) Pourbaix, M. *Atlas of Electrochemical Equilibria in Aqueous Solutions*, 2nd ed..; National Association of Corrosion: Houston, TX, 1974.
(38) Mills, T. J.; Lin, F.; Boettcher, S. W. Theory and Simulations of Electrocatalyst-Coated Semiconductor Electrodes for Solar Water Splitting. *Phys. Rev. Lett.* **2014**, *112* (14), 148304.
(39) Sze, S. M.; Ng, K. K. *Physics of Semiconductor Devices*, 3rd ed.; Wiley-Interscience: Hoboken, NJ, 2007.
(40) Zhu, W. J.; Ma, T.-P.; Tamagawa, T.; Kim, J.; Di, Y. Current Transport in Metal/Hafnium Oxide/Silicon Structure. *IEEE Electron Device Lett.* **2002**, *23* (2), 97−99.

DOI: 10.1021/acscatal.8b01929
ACS Catal. 2018, 8, 8545−8552